05,12

Structure and magnetic properties of the cobalt-nickel coatings obtained by the chemical deposition method using arabinogalactan as a reducing agent

© S.V. Stolyar[1,3], L.A. Chekanova[2], E.A. Denisova[2], R.N. Yaroslavtsev[1,2], E.V. Cheremiskina[3], I.V. Nemtsev[1,2,3], R.S. Iskhakov[2], I.G. Vazhenina[2,¶], A.A. Matsynin[2], M.N. Volochaev[2], B.G. Sukhov[4]

[1] Federal Research Center Krasnoyarsk Scientific Center of the Siberian Branch of the Russian Academy of Sciences, Krasnoyarsk, Russia
[2] Kirensky Institute of Physics, Federal Research Center KSC SB, Russian Academy of Sciences, Krasnoyarsk, Russia
[3] Siberian Federal University, Krasnoyarsk, Russia
[4] V.V. Voevodsky Institute of Chemical Kinetics and Combustion, Siberian Branch, Russian Academy of Sciences, Novosibirsk, Russia

¶ E-mail: irina-vazhenina@mail.ru

Received April 18, 2024
Revised April 18, 2024
Accepted May 8, 2024

The cobalt-nickel coatings containing carbon were obtained by the chemical deposition method from salt solutions of transition metals using arabinogalaktan as a reducing agent. A crystalline structure and chemical composition of the coatings were detected. Carbon is found to be present in the form of graphite inclusions. Saturation magnetization, field of local anisotropy, and the size of correlation radius of axes of anisotropy were found by magnetic measurements for the coatings synthesized. The measurements carried out by ferromagnetic resonance allowed one to determinate the effective magnetization and the field of perpendicular anisotropy.

Keywords: chemical deposition, magnetic coating, ferromagnetic resonance, magnetization curve, magnetic anisotropy.

DOI: 10.61011/PSS.2024.06.58702.21HH

1. Introduction

The dependence of the properties of binary magnetic alloys on both the composition and the dimensional and morphological parameters of nanostructured objects determines a significant interest in such structures. The materials based on the CoNi alloy have magnetic properties which are important for practical applications in magnetic recording, electromagnetic absorption, biomedicine, etc. [1–5]. Separately, it is worth noting the wide range of morphology of the objects obtained: dendrites [6], powders [4,7,8], films [9], nanotubes [10,11]. Metal coatings are obtained by various technological methods: reduction of the corresponding metals from aqueous solutions of salts (chemical, electrolytic deposition) [12,13], magnetron sputtering [14,15], molecular beam epitaxy [16], solid-phase synthesis [17]. The chemical deposition (CD) method is the simplest and most economically efficient way to apply metal coatings [18]. Coatings can be obtained on both conductive and dielectric surfaces. These coatings demonstrate high hardness and corrosion resistance [19–23]. Therefore, for instance, the nickel coating has acquired the greatest commercial importance among coatings produced by the chemical method [19]. The CD process is autocatalytic, metal ions are reduced in solution by oxidation of the reducing agent. This process requires reduction of the cation of the deposited metal by receiving electrons from the substrate surface. The reducing agent, in turn, supplies electrons to this surface and is thus oxidized.

Such compounds as hypophosphite, borohydride, and hydrazine are usually used as a reducing agent. The reducing agents used will determine the magnetic properties of the synthesized coatings. In the case of hypophosphite, metal coatings $Me_{1-x}P_x$ are substitutional solid solution (at phosphorus concentration of $x < 10$ at.%). The presence of phosphorus reduces the saturation magnetization of the alloy. The experience of usage of natural polysaccharides [24–26] as a reducing agent makes them promising for chemical precipitation. The polysaccharide arabinogalactan of Siberian larch was used in this study as a reducing agent for the preparation of ferromagnetic metal coatings of 3d metals. The arabinogalactan molecule consists of galactose and arabinose units. The respective monosocharides have an aldehyde group with reducing properties. The production of metal nanoparticles using arabinogalactan from salts of noble metals (Au, Ag, Pd, Pt, etc.) was implemented in Ref. [27].

This work is devoted to the preparation and study of the crystal structure, electrical and magnetic (static, dynamic)

properties of CoNi coatings obtained by chemical deposition using arabinogalactan as a reducing agent.

2. Experimental method

Aqueous solutions of cobalt sulfate and nickel sulfate were used to obtain ferromagnetic coatings of 3*d*-metal alloys. Arabinogalactan isolated from larch was used as a reducing agent. Sodium citrate and trilone B were chosen as the complexing agent and stabilizer, respectively. The coatings were deposited on copper foil, cover glasses, and polycrystalline glass. The thickness of coating on the copper foil was several microns, the thickness of coating on the cover glasses was ~ 50 nm. The surface of glass substrates and polycrystalline glass was pre-activated in solutions of $PdCl_2$ and $SnCl_2$ to create metal reduction and crystallization centers [28]. Ammonium hydroxide is added to the resulting solution until the pH of the solution reaches 11. Deposition was carried out at a temperature of 80°C. The required temperature was maintained using the water thermostat TZh-TS-01. The deposition rate was determined based on the increase of the mass of the substrate during the formation of the coating. The obtained magnetic metal coatings were studied using transmission electron microscope Hitachi NT7700 (accelerating voltage 110 kV) and scanning electron microscope CarlZeiss EVO 60. Elemental mapping using energy dispersive X-ray spectroscopy was used to characterize the chemical composition of the CoNi alloy. The structural analysis was performed using X-ray diffractometer DRONE-4. The structural and phase transitions was studied during sample heating by observing changes of the material electrical resistance $R(T)$ using the four-probe method. This method is characterized by simple application, continuity of the process and the possibility of visual observation of the processes taking place. $R(T)$ was measured in a vacuum of the order of 10^{-6} Torr, using a molybdenum heating element and an ADC-LCard-E14-440. The temperature was controlled using a K-type thermocouple. All elements (sample, probes, thermocouple) were positioned on a 5 mm thick copper plate for uniform heating and cooling.

Static and dynamic magnetic measurements were carried out at room temperature on a vibrating magnetometer and a standard spectrometer EPR-2M, respectively. The absorption spectra of ferromagnetic resonance (FMR) were measured at a resonator pumping frequency of 9.2 GHz.

Static magnetic measurements were performed along and perpendicular to the coating plane. Information about the characteristics of local magnetic anisotropy is contained in the saturation magnetization curves [29], which is described by the expression

$$M(H) = M_0\big(1 - 2d_M(H)\big)^{1/2}, \qquad (1)$$

where d_M — relative dispersion of fluctuations of transverse magnetization components, M_0 — saturation magnetization

$$d_M = \frac{DH_a^2}{2H^{1/2}(H_l^{1/2} + H^{1/2})^3}. \qquad (2)$$

$D^{1/2}H_a$ is the rms fluctuation of the local anisotropy field in this expression. The correlation field $H_l = 2A/Mr_l^2$, also defined as the exchange field, is an auxiliary characteristic that contains information about the correlation radius of the axis of local anisotropy r_l (in nanostructure $2r_l$ is equal to the size of the crystallite). As can be seen from (2) in the domain $H \ll H_l\, d_M \sim H^{-1/2}$ (i.e. $M(H)$ is determined by cooperative effects), and in the domain $H \gg H_l\, d_M \sim H^{-2}$ (i. e. $M(H)$ is determined by Akulov's law), a crossover is observed in the vicinity of $H = H_l$ consisting in a change of the dependence of the curve $d_M(H)$ from $H^{-1/2}$ to H^{-2}. Knowing the numerical value of the exchange constant A, it becomes possible, to calculate the values of the correlation radii r_l of the produced coatings using the measured value of the correlation field H_l.

The FMR method allows determining several macroscopic magnetic parameters: effective magnetization M_{eff}, field of perpendicular anisotropy H_{an}, field of anisotropy in the plane $H_{\|}$.

The expression of the FMR resonant frequency FMR ω_0 in the spherical coordinate system [30–32] can be presented as follows through the total energy of the magnetic system E

$$E = -MH\lfloor \sin\theta \sin\theta_H \cos(\varphi - \varphi_H) + \cos\theta \cos\theta_H \rfloor + [2\pi M^2 + K_n]\cos^2\theta + K_u \sin^2\theta \sin\theta^2(\varphi - \varphi_0) \qquad (3)$$

when the equilibrium position of the magnetization vector and the free energy density [31] is determined by the relations

$$\frac{\partial E}{\partial \varphi} = \frac{\partial E}{\partial \theta} = 0, \qquad (4)$$

taking into account the Landau-Lifshitz equation for the motion of magnetization M, given by polar θ and azimuthal φ angles

$$\omega_0 = -\frac{\gamma}{M\sin\theta}\left[\frac{\partial^2 E}{\partial\theta^2}\frac{\partial^2 E}{\partial\varphi^2} - \left(\frac{\partial^2 E}{\partial\theta\partial\varphi}\right)^2\right]^{1/2}. \qquad (5)$$

In the expressions above $\gamma = 1.758 \cdot 10^7$ Hz/Oe — gyromagnetic ratio, K_n — constant of perpendicular uniaxial anisotropy; K_u — constant of uniaxial anisotropy in the plane, φ_0 — direction of the uniaxial anisotropy field in the plane, θ_H and φ_H — angles describing the position of the internal field vector. It should be noted that the first and second constants of cubic anisotropy in the expression (3) are assumed to be equal to zero.

3. Experimental results

The TEM image of the coating on a glass substrate, shown in Figure 1, *a*, demonstrates a structure of the type

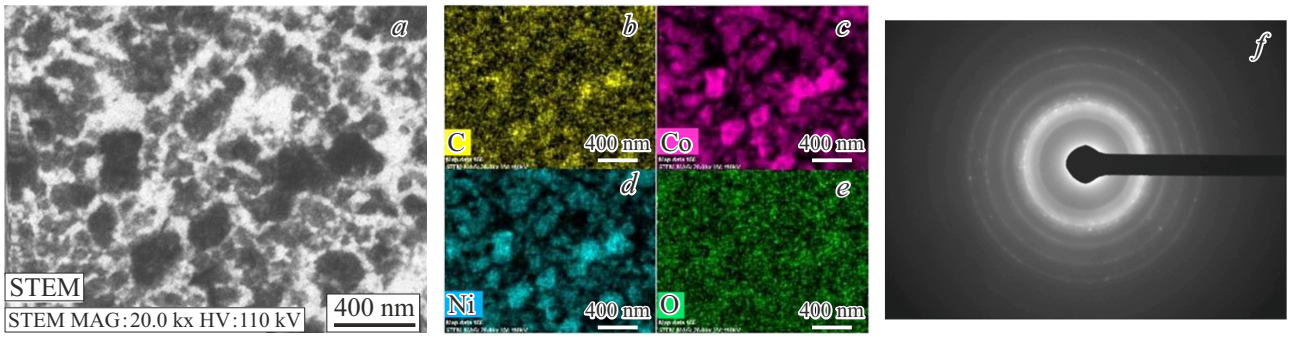

Figure 1. TEM image of the coating (*a*) and X-ray mapping of the surface (*b, c, d, e*). Microdifraction pattern (*f*).

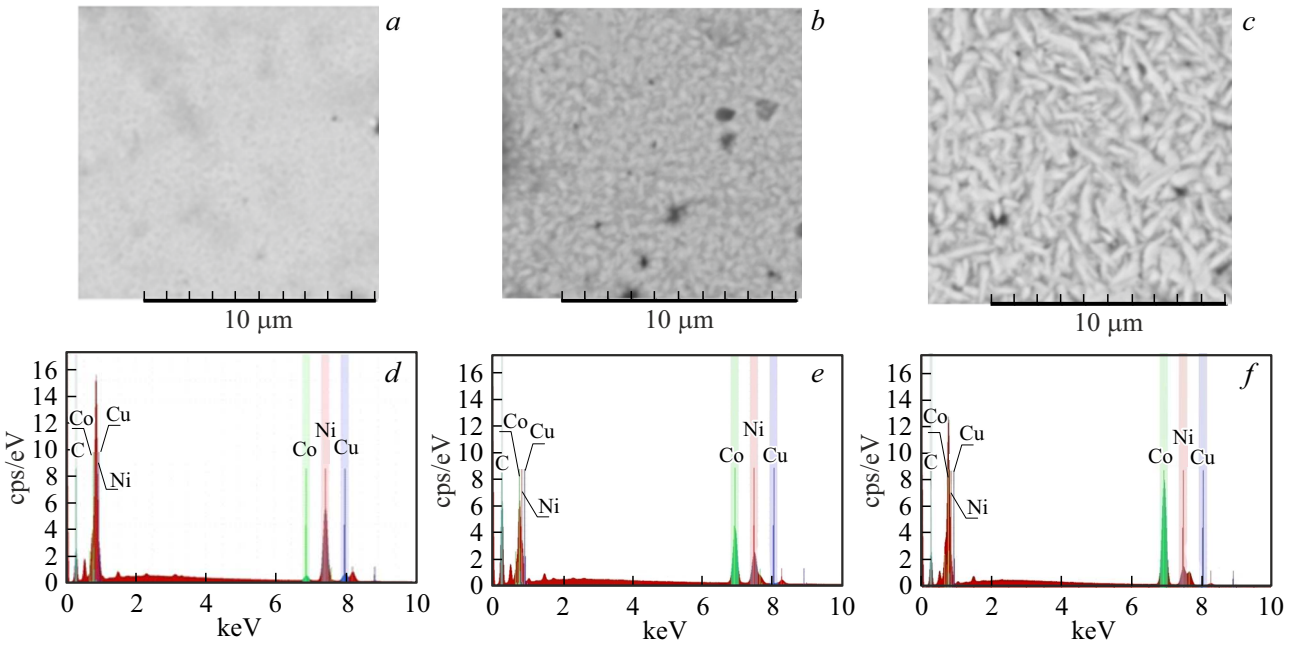

Figure 2. Images of three samples obtained using a scanning electron microscope: *a* — Co_5Ni_{95}, *b* — $Co_{60}Ni_{40}$, *c* — $Co_{80}Ni_{20}$, as well as energy spectra with the distribution of elements in these samples (*d, e, f*).

„salt-pepper“ [33] with visible conglomerates of nanoparticles with a size of 100–400 nm. Figure 1, *b, c, d, e* also shows the distribution of detected chemical elements (C, Co, Ni, O) obtained by energy-dispersive X-ray analysis. Elemental analysis showed that the metal phase in this sample is mainly represented in nanoparticle conglomerates and has the composition of $Co_{63}Ni_{37}$. It is also determined that there is an admixture of carbon, but this method does not accurately estimate its amount (as well as an evenly distributed admixture of oxygen). The electrogram (Figure 1, *f*) indicates the absence of texture in the produced alloy.

SEM images of coatings of various compositions on a copper substrate, as well as the distribution of elements obtained by energy dispersive X-ray analysis, are shown in Figure 2. The images show that with an increase of the cobalt content in the alloy, the coatings become more textured. Characteristic elongated formations are observed in Figure 2, *c*, located in the coating plane with a microstructure of the „vermicelli“ type. Elemental analysis showed that the metal coating consists of nickel and cobalt with an admixture of carbon (Figure 2, *d, e, f*).

Figure 3 shows the results of X-ray phase analysis of $Co_{1-x}Ni_x$ alloy coatings on a copper substrate. X-ray images show both reflections corresponding to a ferromagnetic alloy and reflections corresponding to a copper substrate. The results of X-ray phase analysis showed the presence of FCC and HCP phases in the magnetic alloy, and an increase of the cobalt content in the alloy correlated with an increase of the intensity of reflections of the HCP phase. The figure shows that the coatings of Co_5Ni_{95} and $Co_{60}Ni_{40}$ the composition characterized by a FCC atomic structure. Coatings of Co and $Co_{80}Ni_{20}$ alloys demonstrate reflections with 2Θ equal to 41 and 75°, which are characteristic of reflections of (100) and (110) HCP atomic structure.

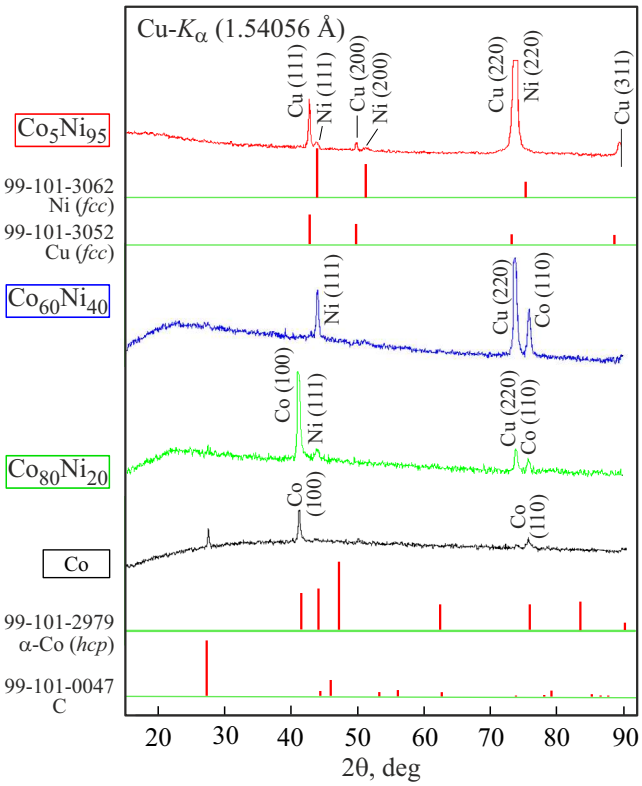

Figure 3. X-ray images of the obtained samples (the numbers on the left side indicate the numbers of the element cards from the ICDD database, after the element symbol, Miller indexes are specified in parentheses).

However, there are no reflections from the family of densely packed planes (002) of the HCP. Therefore, the formed HCP alloy structure is textured. The axis z is located in the coating plane. The calculated atomic lattice constants of the recorded FCC and HCP structures correspond to the values characteristic of the $Co_{1-x}N_{xi}$ alloy, which suggests the absence of a solid metal-carbon solution. Low-intensity reflections were recorded on some radiographs of freshly prepared samples at $2\Theta = 27°$ (Figure 3). This reflection is caused by reflections from densely packed planes of the graphite phase. This indicates that the carbon impurity crystallizes into graphite inclusions. Any reflections characteristic of carbides (Co_2C, Ni_2C, Co_3C, Ni_3C) were not detected. The absence of carbides is also indicated by the magnetic properties of the studied coatings.

Structural and phase transitions are often manifested by changes of electrical resistance, the latter allows for accurate measurements of the temperature of these transitions (and for estimation of the rate of the process). Figure 4 shows the forward and reverse course of the dependence of the electrical resistance $R(T)$ on the temperature of $Co_{80}Ni_{20}$ coating on a polycrystalline glass. These dependences indicate the metallic nature of the conductivity of the studied coatings (sign of temperature coefficient of resistance). A singularity (inflection point) is observed at $T = 250°C$ on the curve $R(T)$ describing the heating of the coating, and a break is observed at $T = 430°C$. A singularity is observed at $T = 400°C$ in the measured range on the cooling curve $R(T)$. These singularities are related both to polymorphic transformations of the crystal structure of the HCP $\leftrightarrow$ FCC type during heating and cooling of the alloy coating (as suggested by the observed temperature hysteresis), and to modification of the nanostructure of the initial coating (recrystalization).

The ferromagnetic resonance method was used to identify the morphological features of the obtained alloys on a glass substrate, as well as to study their magnetic properties.

The calculated the angular dependence of the resonant field quite close to the experimental values was obtained by numerically solving the system of equations (3)–(5) for the given values of the perpendicular anisotropy field ($2K_n/M_S$), the anisotropy field in the plane ($H_{an} = 2K_u/M_S$) and the effective magnetization M_{eff} (Figure 5). The angular

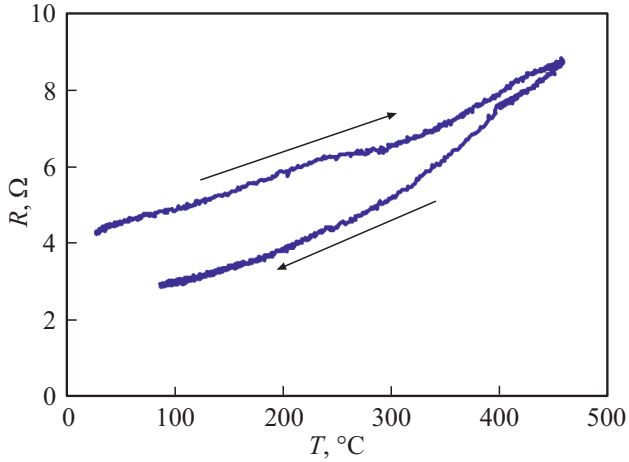

Figure 4. Temperature dependence of the electrical resistance of $Co_{80}Ni_{20}$ coating obtained on a polycrystalline glass.

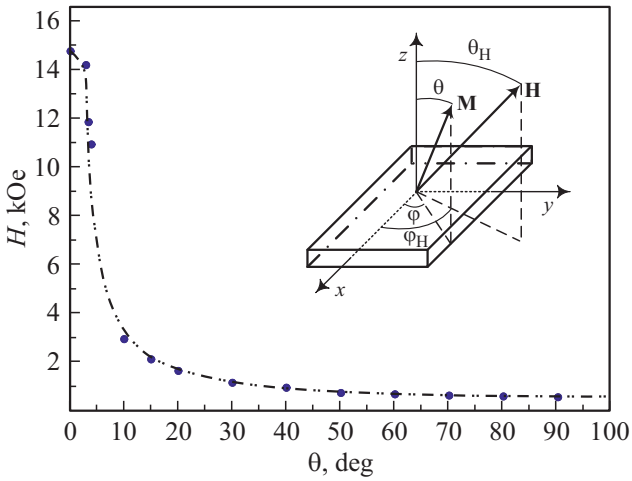

Figure 5. The angular dependence of the FMR resonance field for $Co_{63}Ni_{37}$ coating, where the dots show the experimental values, and the dotted line shows the calculated curve. The inset shows a diagram illustrating the geometry of the experiment.

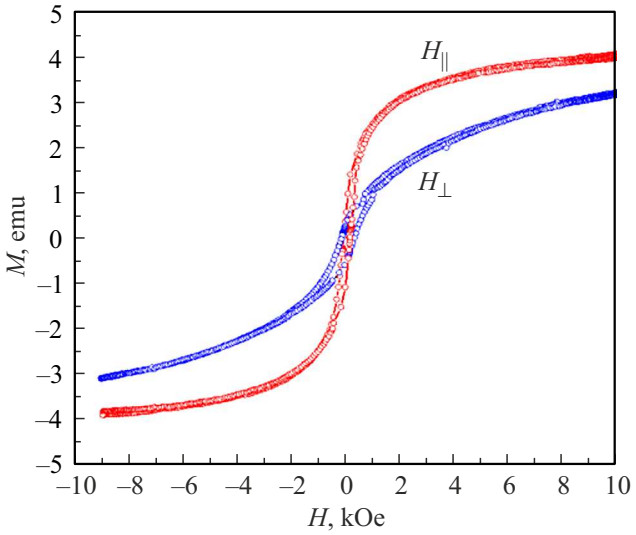

Figure 6. Hysteresis loops of $Co_{80}Ni_{20}$ coating measured in two geometries (along $H_{\parallel}$ and perpendicular to $H_{\perp}$ plane of the coating).

dependence is characteristic of a planar magnetic coating. Based on the results of FMR measurements it was found that the value of the anisotropy field in the plane is zero when the angle φ_H changes. The calculated curve allowed determining the values of M_{eff} and H_{an}, which amounted to 1100 G and 5800 Oe, respectively. The obtained magnetization value matches the known value for the alloy $Co_{63}Ni_{37}$ prepared using other methods [9,34–36]. The width of line ΔH, estimated at values θ_H 0 and 90°, was 350 Oe.

Figure 6 shows the hysteresis loops of $Co_{80}Ni_{20}$ coating (on a copper substrate) measured in two geometries (along and perpendicular to the coating plane) in the field range from 0 to 10 kOe at room temperature. The appearance of the magnetization curves suggests the anisotropy of the shape of the studied coating.

The analysis of magnetization curves measured in parallel orientation to (1)–(2), taking into account the numerical value of the exchange interaction constant A, the values of which for $Co_{1-x}Ni_x$ alloys were repeatedly determined both by the spin-wave resonance method and using the low-temperature magnetization path according to Bloch's law $(M(T) = M_0(1 - BT^{3/2}))$ [9,34–37] allowed calculating the values of the correlation radii r_l of the produced coatings (using the value of the exchange field). The values of saturation magnetization M_0, coercive force H_c, correlation field H_l, and correlation radii r_l are listed in the table.

Magnetic parameters of coatings

	M_0, G	$D^{1/2}H_a$, kOe	H_l, Oe	r_l, Å	H_c, Oe
Co_5Ni_{95}	590	0.70	2235	65	70
$Co_{40}Ni_{60}$	1180	0.76	3730	67	63
$Co_{58}Ni_{42}$	1060	1.28	3465	73	50
$Co_{80}Ni_{20}$	1250	2.20	5180	68	67

4. Discussion

Coatings of ferromagnetic alloys were obtained from aqueous solutions of Co and Ni salts in the presence of arabinogalactan polysaccharide. The formation of a metal coating is probably attributable to the oxidation-reduction interaction on the electrically conductive surface of a metal substrate, or on conductive metal palladium nuclei previously created on the non-conductive surface of a glass or polycrystalline glass substrate by pretreatment of $PdCl_2$ and $SnCl_2$. Obviously, the diffusion to the conductive layer of the substrate of oxidizing agents, i.e. metal cations, in a highly alkaline (pH = 11) aqueous-ammonia medium takes due to their transformation into water-soluble complex ammoniacates of cobalt and nickel under these conditions. Water-soluble macromolecules of arabinogalactan themselves can act as diffusion-mobile reducing agents, having reducing terminal monosaccharide units capable of opening with the formation of reducing aldehyde groups. The latter are oxidized to acyl radicals and then to carboxyl groups, which in turn, with further redox interaction with a metal cation, are able to oxidize further to carboxyl radicals decarboxylating with the relase of CO_2 and generation of carbon-centered radicals on macromolecules [38]. The latter can both oxidize even deeper to carbocation centers, which turn into secondary alcohol groups in an alkaline medium, and recombine with each other, forming new associated intermacromolecular structures with new carbon-carbon bonds (which is important for understanding the formation of the carbon-carbon graphite phase). Moreover, arabinogalactan macromolecules, like other hemicelluloses, can be subjected to alkaline peeling in highly alkaline conditions, i.e. stepwise exhaustive defragmentation from one monosaccharide unit to another with the formation of small organic reducing fragments [39]. The latter in the similar scenario are capable of producing carbon-centered radicals both participating further in the oxidation chain and recombining with each other to form carbon-carbon bonds in the single-electron oxidation conditions. Therefore, arabinogalactan oxidation products with new carbon-carbon bonds will accumulate on the metal surface in addition to the growth of the metal phase as the oxidation-reduction interaction of metal cations with arabinogalactan macromolecules and products of its alkaline defragmentation proceeds on this surface. Apparently, the oxidation of a polysaccharide on an electrically conductive substrate is not limited to the proposed reactions, since the final solid-phase product of the polysaccharide transformation is graphite, which is detected by X-ray phase analysis.

The phase composition of the produced coatings is characterized by densely packed metal structures characteristic of the phase diagram of $Co_{1-x}Ni_x$ alloys. Ni-based alloys

are characterized by a FCC structure, while Co-based alloys have an anisotropic HCP structure. In the initial state, the obtained coatings are heterophase and consist of a mechanical mixture of a solid solution of $Co_{1-x}N_{xi}$ and graphite. It is possible to use the analysis of possible variants of Hornbogen microstructures to identify the nature of the spatial distribution of the detected phases [40]. 4 types of microstructure can be realized in a two-phase alloy according to his classification. (1) — A dispersed microstructure characterized by the fact that dispersed graphite inclusions are located in a matrix consisting of a solid solution of $Co_{1-x}Ni_x$. (2) — A variant of the cellular microstructure in which the crystallites of the $Co_{1-x}Ni_x$ phase are assembled into blocks of size $L \gg r$ (where r — the size of the crystallite). In this case, the graphite phase is the matrix. (3) — The phases are distributed continuously relative to each other in the case of a two-frame microstructure, so the flow exists in both phases. (4) — The layered modulated microstructure is formed by extended single-phase layers. The results of measurements of electrical resistance $R(T)$ suggest the existence of a flow through the metal component of a heterophase coating, therefore, the presence of a cellular microstructure can be excluded. Measurements performed using the ferromagnetic resonance method indicate anisotropy of the shape of the formed magnetic formations in case of formation of the coating. The given angular dependences of the resonant fields (Figure 5) are typical for the case of a plate, and certain values of magnetization are consistent with the chemical composition. The anisotropy of the hysteresis loops depending on the direction of the magnetic field relative to the film plane also suggests a thin plate model. Therefore, it is possible to exclude the variants of the dispersed and two-frame microstructure of the obtained coatings based on the results of FMR and $M(H)$. The saturation magnetization M_0 of the produced coatings, determined by the FMR method and using magnetization curves, correlates with changes in chemical composition and is consistent with the literature data. The magnitude of the anisotropy field increases with an increase of the Co content in alloys. So, for the coating of composition $Co_{40}Ni_{60}$ $D^{1/2}H_a = 0.76\,\text{kOe}$, for the coating $Co_{80}Ni_{20}$ $D^{1/2}H_a = 2.2\,\text{kOe}$. The change of the anisotropy field is a consequence of a change of the phase composition of coatings with an increase of the Co content — an increase of the proportion of the HCP phase. The correlation radius r_l, which characterizes the spatial uniformity of the local anisotropy field in the manufactured crystalline coatings, in this case, can be identified with the size of the crystalline grain. The size does not depend on the chemical composition of the alloy and equals to $\sim 7\,\text{nm}$. The magnitude of the coercive field of the manufactured coatings, which is several tens of oersteds, does not depend on the chemical composition (see the table). This makes it possible to consider the manufactured alloys as magnetically soft nanocrystalline, with pronounced exchange correlations, in which the grains are assembled into conglomerates with dispersed inclusions of the graphite phase at the boundaries of the conglomerates or at their triple joints.

5. Conclusion

Ferromagnetic coatings of Co_5Ni_{95}, $Co_{58}Ni_{42}$, $Co_{60}Ni_{40}$, $Co_{63}Ni_{37}$, $Co_{80}Ni_{20}$ compositions were obtained on conductive and dielectric surfaces by chemical deposition. Arabinogalactan polysaccharide isolated from Siberian larch was used as a reducing agent. The graphite inclusions are present in the ferromagnetic alloy $Co_{1-x}Ni_x$ according to structural measurements.

The temperature dependence of the electrical resistance indicates the metallic nature of the conductivity of the studied coatings (positive temperature coefficient of resistance). The shape of the curves and the recorded singular dots are associated both with polymorphic transformations of the crystal structure of the HCP $\leftrightarrow$ FCC type in case of heating and cooling of the alloy coating (as indicated by the observed temperature hysteresis), and with modification of the nanostructure of the initial coating (recrystalization).

Static $M(H)$ and dynamic (FMR) magnetic measurements of produced CoNi alloys allowed determining the magnetic parameters: saturation magnetization M_0, coercive force H_c, correlation field H_l, correlation radii r_l, the field of perpendicular anisotropy $H_\perp$, the field of anisotropy in the plane $H_\parallel$. The dependence of the magnetization on the composition indicates the absence of a solid metal-carbon solution. Produced nanocrystalline coatings demonstrate magnetically soft properties at room temperature.

Therefore, the results of the work demonstrate the possibility of synthesis by chemical deposition of metal coatings using arabinogalactan as a reducing agent. Structural and magnetic studies indicate that carbides are not formed.

Acknowledgments

The authors would like to thank the Krasnoyarsk Regional Center of Research Equipment of Federal Research Center „Krasnoyarsk Science Center SB RAS“ equipment provided for measurements.

Funding

The work was carried out within the scientific scope of the state assignment of the Federal Research Center „Krasnoyarsk Scientific Center of the Siberian Branch of the Russian Academy of Sciences“.

Conflict of interest

The authors declare that they have no conflict of interest.

References

[1] A. Masoero, B. Morten, G.L. Olcese, M. Prudenziati, F. Tango, F. Vinai. Thin Solid Films **350**, 214 (1999).
[2] G.D. Hibbard, K.T. Aust, U. Erb. Mater. Sci. Eng. A **433**, 195 (2006).
[3] T. Onoue, M.H. Siekman, L. Abelmann, J.C. Lodder. JMMM **287**, 501 (2005).
[4] G.V. Kurlyandskaya, S.M. Bhagat, C. Luna, M. Vazquez. J. Appl. Phys. **99** (2006).
[5] O. Ergeneman, K.M. Sivaraman, S. Pané, E. Pellicer, A. Teleki, A.M. Hirt, M.D. Baró, B.J. Nelson. Electrochim. Acta **56**, 1399 (2011).
[6] M. Yasir Rafique, L. Pan, A. Farid. J. Alloys Compd. **656**, 443 (2016).
[7] D. Mercier, J.-C.S. Lévy, G. Viau, F. Fiévet-Vincent, F. Fiévet, P. Toneguzzo, O. Acher. Phys. Rev. B **62**, 532 (2000).
[8] D.A. Bizyaev, A.A. Bukharaev, N.I. Nurgazizov, A.P. Chuklanov, A.R. Akhmatkhanov, V.Y. Shur. Ferroelectrics **574**, 65 (2021).
[9] P. Talagala, P.S. Fodor, D. Haddad, R. Naik, L.E. Wenger, P.P. Vaishnava, V.M. Naik. Phys. Rev. B **66**, 144426 (2002).
[10] Y. Rheem, B.-Y. Yoo, W.P. Beyermann, N.V. Myung. Nanotechnology **18**, 125204 (2007).
[11] T. da Câmara Santa Clara Gomes, J. De La Torre Medina, M. Lemaitre, L. Piraux. Nanoscale Res. Lett. **11**, 466 (2016).
[12] S.S. Djokić. Fundamentals of Electroless Deposition. In: Encycl. Interfacial Chem. Elsevier (2018). P. 161–173.
[13] A. Lahiri, G. Pulletikurthi, F. Endres. Front. Chem. **7** (2019).
[14] A.V. Svalov, V.E. Ivanov, C.V. Andreev, V.N. Lepalovsky, A.A. Feshchenko, E.V. Kudyukov, I.A. Makarochkin, G.V. Kurlandskaya. FTT **65**, 894 (2023).
[15] F. Wang, J. Wu. Magnetron sputtering. In: Mod. Ion Plat. Technol. Elsevier (2023). P. 189–228.
[16] M.A. Herman, W. Richter, H. Sitter. Molecular Beam Epitaxy. (2004). P. 131–170.
[17] L.E. Bykova, V.G. Myagkov, I.A. Tambasov, O. Bayukov, V.S. Zhigalov, K.P. Polyakova, G.N. Bondarenko, I.V. Nemtsev, V.V. Polyakov, G.S. Patrin, D.A. Velikanov. FTT **57**, 366 (2015). (in Russian).
[18] A. Brenner, G.E. Riddell. J. Res. Natl. Bur. Stand. **37**, *1*, 3134 (1946).
[19] J. Sudagar, J. Lian, W. Sha. J. Alloys Compd. **571**, 183 (2013).
[20] R.N. Yaroslavtsev, L.A. Chekanova, S.V. Komogortsev, R.S. Iskhakov. Solid State Phenom. **215**, 237 (2014).
[21] R.S. Iskhakov, S.V. Komogortsev, A.D. Balaev, L.A. Chekanova. Pisma v ZhTF **28**, *17*, 725 (2002). (in Russian).
[22] R.C. Agarwala, V. Agarwala. Sadhana **28**, 475 (2003).
[23] K.G. Keong, W. Sha. Surf. Eng. **18**, 329 (2002).
[24] S. Machado, S.L. Pinto, J.P. Grosso, H.P.A. Nouws, J.T. Albergaria, C. Delerue-Matos. Sci. Total Environ. **445–446**, 1 (2013).
[25] W. Lu, C. Ou, P. Huang, P. Yan, B. Yan. Int. J. Electrochem. Sci. **8**, 8218 (2013).
[26] V.V. Shulikov, A.P. Potapov. Nanotekhnika **4**, 66 (2012). (in Russian).
[27] E.R. Gasilova, G.N. Matveeva, G.P. Aleksandrova, B.G. Sukhov, B.A. Trofimov. J. Phys. Chem. B. **117**, 2134 (2013).
[28] R.D. Fisher, W.H. Chilton. J. Electrochem. Soc. **109**, 485 (1962).
[29] V.A. Ignatchenko, R.S. Iskhakov, G.V. Popov. ZhETF **55**, *5*, 878 (1982). (in Russian).
[30] H. Suhl. Phys. Rev. **97**, 555 (1955).
[31] J. Smit, H.G. Beljers. Philips Res. Repts **10**, 113 (1955).
[32] J.O. Artman. Phys. Rev. **105**, 74 (1957).
[33] A.M. Glezer, N.A. Shurygina. Amorfno-nanokristallicheskiye splavy. Fizmatlit, M. (2013). 452 s. (in Russian).
[34] I.G. Cullis, M. Heath. J. Phys. F Met. Phys. **10**, 309 (1980).
[35] D.P. Mitra, J.S.S. Whiting. J. Phys. F Met. Phys. **8**, 2401 (1978).
[36] S.V. Komogortsev, R.S. Iskhakov, K.A. Shaikhutdinov, V.K. Mal'tsev, A.V. Okotrub, A.G. Kudashov, U.V. Shubin. Phys. Met. Metallogr. **102**, S67 (2006).
[37] C. Kittel. Phys. Rev. **110**, 1295 (1958).
[38] M.V. Lesnichaya, B.G. Sukhov, G.P. Aleksandrova, E.R. Gasilova, T.I. Vakul'skaya, S.S. Khutsishvili, A.N. Sapozhnikov, I.V. Klimenkov, B.A. Trofimov. Carbohydr. Polym. **175**, 18 (2017).
[39] B.A. Trofimov, B.G. Sukhov, V.V. Nosyreva, A.G. Mal'kina, G.P. Aleksandrova, L.A. Grishchenko. Dokl. Chem. **417**, 261 (2007).
[40] E. Hornbogen. J. Mater. Sci. **21**, 3737 (1986).

Translated by A.Akhtyamov